BMC Veterinary Research

RESEARCH

Open Access

In vitro evaluation of anthelmintic activity of biocompatibile carbon quantum dot nanocomposite against egg and larval stages of equine strongyles

Armin Fakheri[1], Bijan Esmaeilnejad[1*], Hamid Akbari[2] and Rahim Molaei[3]

Abstract

Background Strongyle nematodes pose a major challenge in veterinary parasitology, causing significant economic losses in livestock due to resistance to conventional treatments. Current anthelmintics, like Ivermectin, often encounter resistance issues. This study aims to address these gaps by synthesizing Carbon Quantum Dots (CQDs) and Copper-Doped CQDs (Cu@CQDs) using glucose extract, and evaluating their nematicidal properties against strongyles in vitro. We assessed the nematicidal effects of CQDs and Cu@CQDs through larval feeding inhibition of first-stage larvae (L1), egg hatch inhibition (EHI), and the mobility and mortality of infectious larvae (L3s). Additionally, we conducted ultrastructural examinations of eggs and larvae and evaluated oxidative/nitrosative stress indicators, including total antioxidant status (TAS), protein carbonylation (PCO), lipid peroxidation (MDA), and oxidative DNA damage in homogenized samples of L3s.

Results The synthesized CQDs displayed semi-spherical morphology with diameters under 30 nm. Cu@CQDs at 12.5 µg/ml achieved over 90% EHI and larval motility inhibition. Fluorescence microscopy confirmed over 90% larval feeding inhibition at the same concentration. Both CQDs and Cu@CQDs induced oxidative stress, indicated by decreased TAS and increased MDA, PCO, and oxidative DNA damage. Scanning Electron Microscopy showed that CQDs and Cu@CQDs penetrated the larvae cuticle, altered the tegument, caused larval mortality, and resulted in egg deformities.

Conclusions Given the potential for resistance to Ivermectin, seeking suitable alternatives is essential. Cu@CQDs exhibit effects similar to Ivermectin, indicating their potential as novel antiparasitic agents against strongyles. These findings emphasize the importance of exploring alternative treatments to address resistance and enhance nematode control efficacy.

Highlights

- Glucose was used to synthesize carbon quantum dots.
- Carbon dots revealed anthelmintic activity.

*Correspondence:
Bijan Esmaeilnejad
b.esmaeilnejad@urmia.ac.ir

Full list of author information is available at the end of the article

- Mechanism of anthelmintic activity of carbon dots was demosntated.
- Carbon dots were nontoxic on the L929 fibroblast cell line.

Keywords In vitro, Anthelmintic, Carbon quantum dot, Strongyle, Glucose

Graphical Abstract

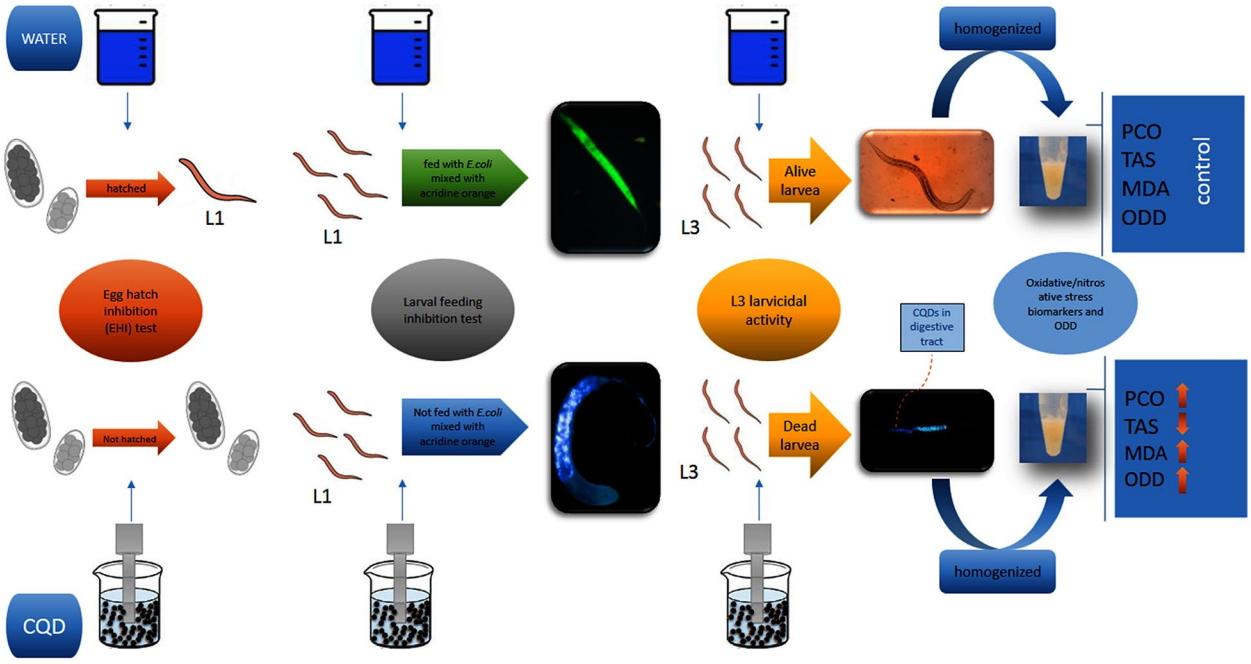

Background

Gastrointestinal parasitic nematodes pose a significant risk to the animal husbandry industry, resulting in substantial economic losses worldwide. Infestations can lead to reduced livestock production, increased treatment costs, stunted growth, and, in severe cases, mortality [1]. It has been estimated that the annual costs associated with gastrointestinal parasitic diseases globally amount to tens of billions of dollars [2], underscoring the severe impact these parasites have on the economy and animal husbandry industry. Hence, it is imperative to implement effective infection control measures to minimize these losses and ensure the sustainability of the livestock industry.

Strongyles belonging to the family Strongylidae, including the large strongyles (*Strongylus*) and small strongyles (cyathostomins), are commonly found internal parasites in equines worldwide [3]. These parasites can cause a range of clinical symptoms in horses, including continuous low-grade fever, anemia, weight loss, reduced hair quality, impaired performance, diarrhea, anorexia, arthritis, colic, and sudden death [4–6].

Resistance to anthelmintics in strongyles, including the large strongyles (*Strongylus*) and small strongyles (cyathostomins), has become a major global concern [3, 7]. Three classes of anthelmintics, including Benzimidazoles, Tetrapyrimidines, and Macrocyclic lactones, are currently used to control strongylosis [8, 9]. However, the emergence of resistance in parasitic worms against conventional anthelmintics has led to the development of new drugs, such as Monepantel and Derquantel, which have been met with limited success and high costs [6, 10]. Equine gastrointestinal nematodes are also affected by anthelmintic resistance. Furthermore, the adverse environmental effects associated with these drugs necessitate the development of alternative treatments.

Carbon quantum dots (CQDs) are nanomaterials with sizes ranging from 1 to 50 nm, which have numerous applications in various fields of science. CQDs are known for their excellent compatibility with the environment [11, 12], good cell penetration [13], high resistance to salt [14], intense fluorescence properties [15], low toxicity and cost-effectiveness [12], making them a promising material for various applications. CQD can be produced by top-down and bottom-up approaches [16]. This classification relies on the size relationship between the CQDs and type of precursor [17]. The bottom-up synthesis of CQDs proceeds through the carbonization of small molecular precursors. When these molecular precursors are pyrolyzed by microwaves or in autoclave, the synthesis readily produces CQDs, highly dispersible in water and displaying remarkable fluorescent properties.

On the contrary, concerning the top-down approaches, the precursors are extended carbon structures or nanostructures, such as graphite, amorphous carbon, carbon fibers, nanotubes, and fullerene, which are chemically or physically stripped, fragmented, or etched to obtain carbon nanoparticles [18].

CQDs have been shown to possess photoelectric properties, making them ideal electron donors and acceptors [14]. Recent studies have investigated the effects of CQDs on microorganisms. For instance, CQDs extracted from henna leaves have been found to have a lethal effect on Gram-negative (*Escherichia coli*) and Gram-positive (*Staphylococcus aureus*) bacteria by damaging the cell wall or producing free radicals, leading to cell death [19]. Similarly, CQDs obtained from vitamin C (VC) have been shown to exhibit antimicrobial properties against *Staphylococcus aureus*, *Bacillus subtilis*, and *Escherichia coli* by sticking to the outer surface of the cell, damaging the cell wall, and causing cell death [20]. Another study has reported that CQDs derived from tamarind and calf thymus DNA (ct-DNA) have a good antibacterial effect against *Klebsiella pneumoniae*, *Escherichia coli*, *Staphylococcus aureus*, and *Pseudomonas aeruginosa* by destroying the bacterial cell wall [11].

CQDs have also been investigated for their antiviral and antifungal properties. One study has demonstrated that CQDs can reduce the infectivity of viruses or induce their inactivation [21]. Moreover, CQDs have been found to exhibit broad-spectrum antifungal activity against various fungi species, such as *R. solani* and *P. grisea* [20]. In addition, CQDs and their conjugates have the potential to be used as antifungal agents against *Candida albicans* [22]. A study has also shown that CQDs inhibit the growth of yeast cells and cause significant changes in their morphology [23]. Furthermore, combining nanoscale carbon with Zinc sulfide (ZnS) has resulted in nanostructures that are taken up by the hypha of the fungus *Fusarium oxysporum*, with low toxicity against the fungus [21]. These findings suggest that CQDs possess a great potential for use in various biomedical applications.

Despite the CQDs, several studies have been conducted on the effects of nanoparticles on strongyles. For instance a research study was conducted to investigate the impact of silver nanoparticles (AgNPs) on the third-stage larvae (L3) of cyathostomins. The findings of the study indicate that the use of silver nanoparticles resulted in the destruction of the third-stage larval form of the nematode [24].

In recent research, the antiparasitic effects of CQDs and gallium-doped CQDs (Ga@CQDs) have also been studied which attributed this effect to destroy the cell wall of *Leishmania* protozoa [25].

The application of CQDs in parasitology is a relatively new approach. Despite their effectiveness against important organisms, there have been no reports on the anthelmintic activity of CQDs. Given the high prevalence of strongyles in Iran and worldwide, the emergence of drug resistance to current antiparasitic drugs, and the unique properties of CQDs, The principal objective of this investigation is to synthesize CQDs and subsequently conduct a comprehensive characterization of their properties. Subsequently, the study aims to assess the potential anthelmintic effects of these synthesized CQDs against various stages of strongyles.

Materials and methods

Ethics approval and consent to participate

All of the protocols were approved by the Faculty of Veterinary Medicine's Committee on the Ethics of Animal Experiments at Urmia University (IR-UU-AEC-3/73).

CQDs synthesis

CQDs were synthesized using glucose as a carbon source and copper (II) chloride as a modifying agent. A solution containing 1.2 g of glucose dissolved in 150 ml of deionized water was placed in a steel autoclave with a Teflon chamber. For the synthesis of copper-doped CQDs (Cu@CQDs), 0.25 g of copper (II) chloride was added to the glucose solution. The autoclave was heated to 200 °C for 6 h and then allowed to cool to room temperature. The synthesized products were purified using Whatman No. 2 filter paper and centrifuged at 15,000 rpm for 20 min. The final products were freeze-dried for subsequent characterization and testing [26].

Characterization of CQDs

The size, morphology, and zeta potential of the synthesized CQDs were analyzed using Transmission Electron Microscopy (Leo 906 E, Carl Zeiss, Germany) and a Microtrac particle analyzer (Nanotrac wave II, Krefeld, Germany). The absorbance spectrum of the doped CQDs was recorded using a Thermo Scientific NanoDrop spectrophotometer (2000 C, Waltham, USA) over the range of 200–600 nm, 1 nm resolution. Elemental composition was analyzed via X-ray photoelectron spectroscopy (Berlin, Germany), and the chemical structures were examined using Fourier Transform Infrared Spectroscopy (FTIR) using KBr pellet in the range of 450–4000 cm^{-1} and the obtained data have been processed with Omnic software (version 6.0; Thermo Electron, Madison, USA).

Cytotoxicity assay

L929 fibroblast cells, obtained from the Pasteur Institute of Iran, were cultured in Dulbecco's Modified Eagle's Medium (DMEM) supplemented with 10% fetal bovine serum (FBS). The cultures were maintained at 37 °C in a 5% CO2 atmosphere to evaluate the cytotoxicity of various CQD formulations. For the MTT assay, cells were

seeded at a density of 7 × 10^4 cells/mL in 96-well plates and incubated for 24 h. After exposure to varying concentrations of CQDs and Cu@CQDs (1.5625 to 50 µg/ml) for an additional 24 h, MTT reagent was added, and the optical density (OD) was measured at 570 nm using a plate reader (BioTek ELx808, USA) [27]. A comparison of OD values between two wells indicated that higher OD values corresponded to greater numbers of viable cells. Based on this information, CQD cytotoxicity was quantified, and the half-maximal inhibitory concentration (IC50) was determined in µg/mL using the formula:

$$\text{Toxicity}\% = \left(1 - \frac{\text{mean OD of sample}}{\text{mean OD of control}}\right) \times 100.$$

Moreover, cell viability percentage was calculated as: $\text{Viability}\% = 100 - \text{Toxicity}\%$ [27].

Fecal samples

Fecal samples were collected from the rectum of horses aged 1.5 to 5 years in various geographical locations within Tabriz city, between April and August 2023. The horses had not received any anti-parasitic treatment for at least 8 weeks prior to sampling. Samples were transported to the laboratory of parasitology, Veterinary Faculty, Urmia University, under anaerobic conditions. In the laboratory, 10 to 15 g of feces were suspended in half a liter of water and filtered through sieves with pore sizes of 250 µm and 125 µm [28]. The resulting liquid was centrifuged at 200 g for 2 min, and the precipitate was mixed with a sugar-saturated solution to extract strongyle eggs. The eggs were counted, and eggs per gram (EPG) were determined using the McMaster method [29, 30]. Positive fecal samples were cultured, and L3 larvae were isolated after 8 days of incubation at 28 °C [31]. The presence of strongyles was confirmed through morphological examination of the L3 and eggs using light microscopy, focusing on distinct characteristics such as size, shape, and surface texture [32, 33].

Egg hatch inhibition (EHI) test

The EHI test was conducted following established protocols [34] with some modifications. Fresh fecal samples containing a minimum of 100 parasite eggs per gram were adjusted to a concentration of 1 egg per microliter by suspending them in deionized water. The eggs were examined under a light microscope (Olympus, model CH40, Japan) to differentiate between hatched and unhatched eggs. For the experimental procedure, 100 µl of egg suspension were dispensed into each well of 84 plate chamber, followed by the addition of 100 µl of CQDs and Cu@CQDs. Each of the CQDs was tested at four different concentrations, specifically 12.5 µg/ml, 6.25 µg/ml, 3.125 µg/ml, and 1.5625 µg/ml. Negative control samples containing PBS and egg suspension, and positive control samples containing Ivermectin 1% [35] and egg suspension, were included. The plates were incubated for 48 h at 27 °C, after which the hatching process was interrupted by the addition of 10 µL of Lugol's iodine solution. The total number of eggs and L1 was counted using a light microscope, and the percentage of inhibition of egg hatching (%EHI) was calculated using the formula [36, 37]:

$$\%\,\text{EHI} = \left[\frac{\text{number of eggs}}{\text{number of larvae} + \text{number of eggs}}\right] \times 100$$

The experiments were repeated three times for each concentration, as well as for the negative and positive control samples.

Larval feeding inhibition test

In this experiment, the feeding ability of first-stage larvae (L1) was evaluated in the presence of different concentrations of CQDs and Cu@CQDs (12.5, 6.25, 3.125, and 1.5625 µg/ml), following modified established protocols for assessing nematode nutritional activities [38, 39]. The larvae were fed a mixture of lyophilized *Escherichia coli* and acridine orange, a nucleic acid-binding dye that fluoresces green when bound to double-stranded DNA (at 520 nm) and red when bound to single-stranded DNA or RNA (at 650 nm). In accordance with the passage, it is notable that CQDs exhibit strong fluorescent characteristics, appearing blue when examined under a fluorescent microscope at a specific wavelength [40] The experimental procedure involved preparing a solution of *Escherichia coli* (2250 µg/mL) mixed with acridine orange and formaldehyde buffer, followed by a brief incubation. Strongyle eggs were washed and incubated to obtain first-stage larvae, which were then separated using the Baermann funnel technique and adjusted to a concentration of 120 to 150 larvae per 50 µL of deionized water. In 96-well plates, 10 µL of CQDs and Cu@CQDs at the specified concentrations (12.5, 6.25, 3.125, and 1.5625 µg/ml) was added, along with 50 µL of the larval stock solution and 240 µL of PBS. After a 2-hour incubation at 23 °C, 1.5 µL of *Escherichia coli* containing acridine orange was added, and the incubation continued for an additional 2 h [41]. The number of feeding larvae was determined by observing intestinal fluorescence using an inverted fluorescent microscope (Ernst Leitz, GMBH, Wetzler, Germany).

L3 larvicidal activity

To obtain strongyle L3 for the experiment, fecal samples containing eggs were processed according to established protocols [42]. Briefly, 100 g of feces were incubated under aerobic conditions at 28 °C and 80–85% humidity.

After 8 days, larvae were extracted using a Baermann funnel method [43]. The larvae were stored at 7–10 °C until use. The experiment was divided into four groups: a treatment group, which was further divided into two subgroups: CQDs (pure carbon quantum dots, G1p) and Cu@CQDs (doped carbon quantum dots, G1d), a negative control group (G2), and a positive control group (G3), each with three replicates [44]. The treatment groups consisted of 120 L3 mixed with 1 ml of either CQDs or Cu@CQDs at varying concentrations (12.5, 6.25, 3.125, and 1.5625 µg/ml). The negative control included deionized water, while the positive control used Ivermectin 1% solution. After 24 h, the contents were analyzed for larval motility, and the percentage inhibition of larval motility (LMT) was calculated using the formula adapted from Al-Rofaai et al. [45]. The formula employed was:

$$\mathrm{LMT}\ (\%) = \left[\frac{\begin{pmatrix}\text{motility percentage in}\\ \text{the treatment group}\\ -\ \text{motility percentage in}\\ \text{the negative control}\end{pmatrix}}{\begin{pmatrix}100\\ -\ \text{motility percentage in}\\ \text{the negative control}\end{pmatrix}}\right] \times 100$$

Oxidative/nitrosative stress biomarkers

To evaluate potential oxidative/nitrosative stress biomarkers in the context of biomolecule damage, larvae from both treated and untreated groups were selected. Tissue homogenates were prepared after washing with deionized water [46] and analyzed for oxidative and nitrosative indices. Total antioxidant status (TAS) was determined using the ABTS substrate (Randox Laboratories Ltd., Crumlin, UK), with absorbance measured at 570 nm after 10 min. The total nitrate/nitrite content was assessed using the Griess reaction method, following standard procedures [47]. Protein carbonyl (PCO) content was determined using the method of Levine (1985) with 2,4-dinitrophenylhydrazine [48]. Malondialdehyde (MDA) content, as a biomarker of lipid peroxidation, was measured using the method described by Buege and Aust [49], with absorbance read at 535 nm.

Oxidative DNA damage (ODD) assay

To assess oxidative DNA damage (ODD), strongyle L3 were examined in different groups: a treatment group (further divided into CQDs and Cu@CQDs) and a negative control group (PBS solution). The samples were permeabilized in 0.2% Triton X-100 for 5 min. Endogenous peroxidase activity was blocked using a peroxidase blocking solution for 10 min at room temperature in darkness. Nonspecific binding sites were blocked with a ready-to-use superblock solution for 30 min. After washing with TBS (0.1% Tween 20), the samples were incubated overnight at 4 °C with a primary antibody specific for 8-oxodG diluted 1:100. Following additional washes in TBS, samples were incubated with a fluorescent anti-mouse secondary antibody conjugated to Alexa Fluor® 594 for 30 min at room temperature. Cross-sections were counterstained with Acridine to visualize nuclear DNA in green [50]. Fluorescence indicative of DNA damage was observed using a Leitz Dialux 20 microscope (Ernst Leitz GMBH, Wetzler, Germany).

In addition to DNA damage assessment, the chemical structure and surface properties of bio-based CQDs, extracted DNA, and the complex formed between DNA and CQDs were analyzed using FTIR spectroscopy (Thermo Nicolet instrument, Nexus® 670, USA), focusing on the wavenumber range of 4000 –450 cm^{-1}.

Ultrastructural analysis of larvae and eggs using scanning electron microscope (SEM)

Larvae

Following exposure to CQDs and Cu@CQDs, ultrastructural analysis of strongyle L3 was performed using scanning electron microscope (SEM). The larvae were washed in PBS and fixed in 0.1 M cacodylate buffer for 24 h. After additional washing, they were fixed with osmium tetroxide (OsO4) in 0.1 M cacodylate buffer, supplemented with 1.25% potassium ferrocyanide. The samples were then washed with cacodylate buffer and ultrapure water. For SEM preparation, the samples were dehydrated using serial ethanol dilutions (30, 50, 70, 90, 100%) and dried using the critical point method [44]. The dried samples were coated with gold using a Desk Sputter Coater (DSR1, VacCoat) to enhance conductivity for imaging analysis. Gold was sputtered onto the samples to achieve a coating thickness of approximately 45 nm [51]. The coated samples were mounted on a metal plate and observed using a SEM (MIRA3 FEG-SEM, DLS, Nanotorac Wave, Microtrac Co. USA).

Eggs

After exposure to CQDs and Cu@CQDs, ultrastructural analysis of strongyle eggs was conducted using SEM. The eggs from both treatment and control groups were placed in a mixture of 1% (v/v) glutaraldehyde and 4% (v/v) formaldehyde in a 0.15 M Na-phosphate buffer (pH 7.2) for 24 h at 4 °C. The samples underwent dehydration through increasing ethanol concentrations (30, 50, 70, 90, 100%). The egg samples were then fixed onto a slide with gelatin and subsequently coated with gold to enhance

conductivity before observation under SEM (MIRA3 FEG-SEM. DLS, Nanotorac Wave, Microtrac Co. USA) [52].

Statistical analysis

The collected data was subjected to analysis using the SPSS program, specifically version 24.0 (SPSS Inc, Chicago, IL, USA). Statistical analysis was carried out using one-way analysis of variance followed by Tukey post hoc test. The data were submitted to Levene's test for homogeneity of variances. Values were considered to be statistically significant at $P < 0.05$.

Results

Characterization and specialized tests of CQDs

The structural and optical characteristics of the as-synthesized doped CQDs were investigated through UV-visible absorption and visual color analysis under both daylight and UV light (Fig. 1B). The absorption spectrum revealed a band in the deep UV region (~ 223 nm) and a typical peak at ~ 284 nm, which correspond to the π-π* transition of the C = C bond and the sp^2 hybrid conjugated structure of the CQDs. Additionally, a tail-like peak observed between 300 and 350 nm can be attributed to the n-π* transition of the C = O or C = N bonds [53]. Under daylight, the prepared CQDs exhibited a visual brown color, while under UV light, they displayed strong green fluorescence, which can be attributed to the quantum confinement effect of the nano dots [16].

The transmission electron microscopy (TEM) micrograph (Fig. 1A) shows that the Cu@CQDs were synthesized in semi-spherical shapes with dimensions less than 30 nm. The measured zeta potential of -23 mV indicates the particles' tendency to electrostatically repel each other, thus providing a stable dispersed system without aggregation [54].

Based on the XPS results, the elemental composition and surface functional states of the produced doped CQDs were analyzed, as shown in Supplementary Fig. 1. The C1s spectrum (Fig. 2A) displays four peaks at binding energy values of 280.6 eV, 282.7 eV, 289.1 eV, and 290.2 eV, which can be assigned to sp^2 C, C-C/C = C, C = N/C = O, and COOH functional groups, respectively [55]. The deconvoluted N1s spectrum (Fig. 2B) was fitted into three peaks with binding energies at 399.2 eV, 400.3 eV, and 400.8 eV, corresponding to –NH-, -NH_2, and –N = surface functionalities, respectively [56]. Furthermore, the O1s core-level spectrum (Fig. 2C) was split into three key peaks related to C-O (529.1 eV), C-O-H/C-O-C (530.4 eV), and C = O/N = O (531.6 eV) bonds/moieties present at the as-prepared CQD surfaces [55]. Finally, the XPS spectrum obtained in the Cu binding energy region fitted into three characteristic peaks at 932.7 eV, 942.5 eV, and 952.6 eV (Fig. 2D), indicating that Cu occurs in the form of Cu [57]. The XPS result showed the C, O, N, and Cu elemental contents in the synthesized Cu-doped CQDs were 49.63%, 46.59%, 1.52%, and 2.26%, respectively.

FTIR analysis

The FTIR technique was employed to investigate the chemical composition of the CQDs, characterize the structural bonding, and reveal potential bonding interactions between CQDs and DNA. In the FTIR spectrum of the as-synthesized CQDs (Fig. 3A), broad absorption peaks around 3406 cm^{-1} and two sharp overlapping bands at 2975 cm^{-1} and 2911 cm^{-1} are attributed to the bond stretching vibrations of O-H and C-H (methyl and methylene groups), respectively. The bands observed at 1711 cm^{-1}, 1402 cm^{-1}, 1231 cm^{-1}, and 1052 cm^{-1} correspond to the bending vibration of C-H outside the benzene ring, C–O stretching, O-H/C-H bending, and C–OH stretching vibrations, respectively [26]. Notably,

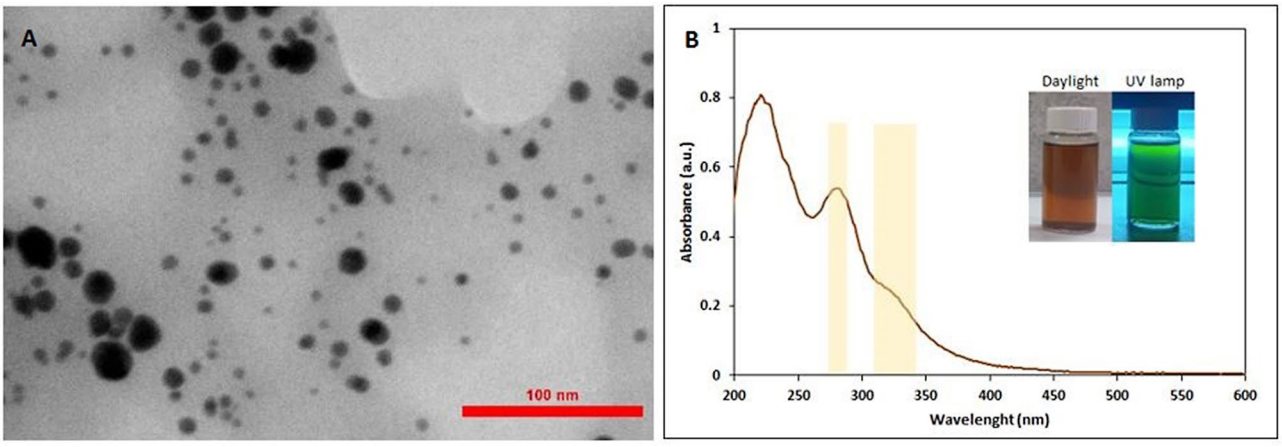

Fig. 1 (**A**) TEM micrographs, and (**B**) absorption spectrum of synthesized Cu-doped CQDs. The color image (inset) shows digital photos of CQDs under Daylight and UV Lamp

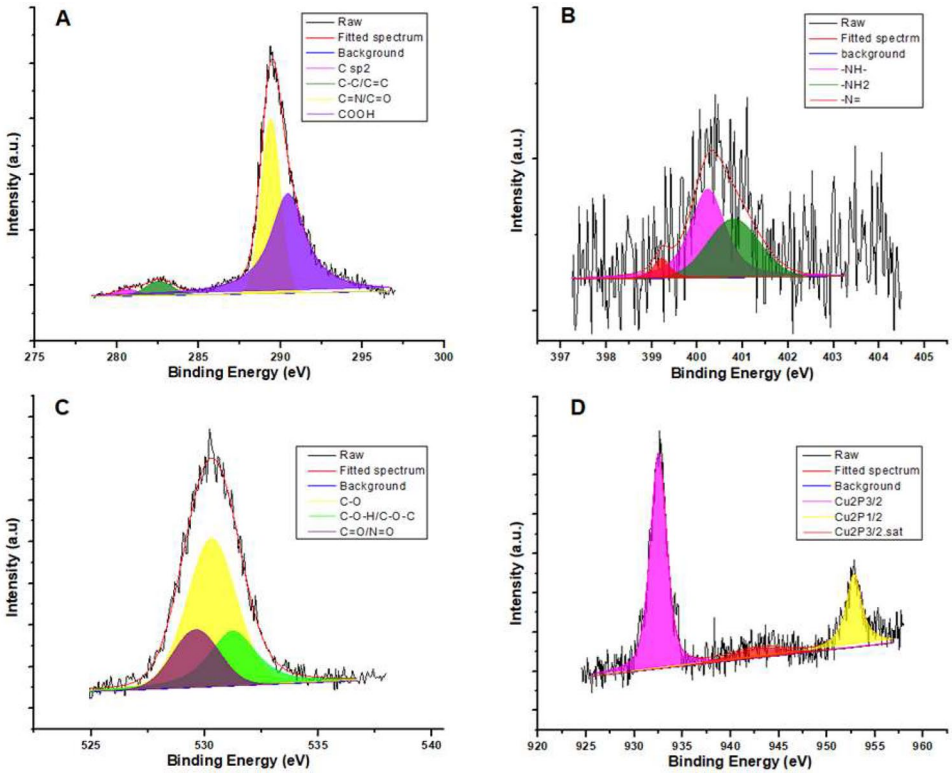

Fig. 2 High-resolution (**A**) C 1s, (**B**) N 1s, (**C**) O 1s, and (**D**) Cu 2P XPS spectra of doped CQDs

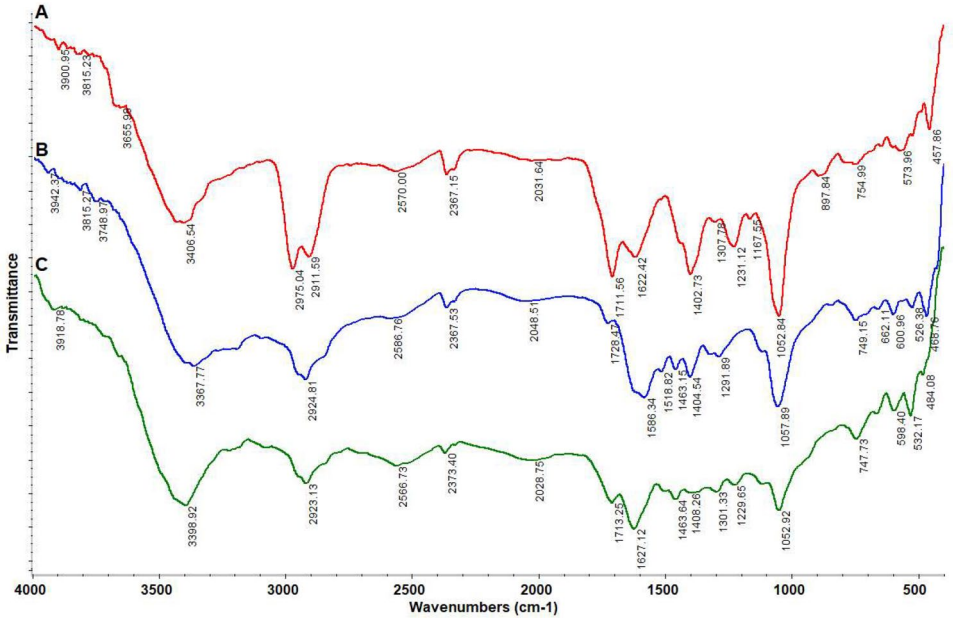

Fig. 3 FTIR spectra of (**A**) CQDs, (**B**) DNA, and (**C**) DNA interacted with CQDs

the peak at 1622 cm^{-1} is attributed to the stretching of C = O bonds [58] which may also indicate the stretching of the Cu–O bond. Additionally, peaks at 457 cm^{-1} and 897 cm^{-1} are assigned to the stretching vibration of Cu–O [59]. The FTIR spectrum of extracted DNA (Fig. 3B) reveals characteristic bands at 3367 cm^{-1} and 1588 cm^{-1}, corresponding to the stretching vibrations of amine groups in the nitrogenous DNA bases and carbonyl groups, respectively. Prominent absorption peaks at 1463 cm^{-1} and 1404 cm^{-1} are associated with the

vibrations of the adenine and guanine rings, respectively. Weak intertwined peaks centered at 1291 cm^{-1} and sharp bands at 1057 cm^{-1} are attributed to the vibrations of the sugar-phosphate backbone (antisymmetric vibrations of phosphate) and deoxyribose (C–O stretch), respectively [60]. It is known that the carbonyl groups of guanine and thymine serve as specific sites for metal-DNA binding. In the spectrum of the interaction between DNA and Cu@CQDs (Fig. 3C), a shift of the carbonyl characteristic bands from 1581 cm^{-1} to 1627 cm^{-1} suggests the tethering of C = O functional groups on DNA with copper atoms from the doped CQDs. Additionally, the shifting of the N-H characteristic peaks in the extracted DNA spectrum from 3367 cm^{-1} to a higher wavenumber (3418 cm^{-1}) and the disappearance of Cu-O absorption peaks after the reaction with as-synthesized CQDs further indicate interactions between DNA and Cu@CQDs [61]. Furthermore, the alteration in both the position and intensity of the antisymmetric vibration of PO_2^- (from 1291 cm^{-1} to 1301 cm^{-1}) serves as additional confirmation of the interaction between DNA and Cu@CQDs, as noted by Rolim et al. [62].

Viability assay

The MTT assay revealed that Cu@CQDs and CQDs exhibited IC50 values of 50 µg/mL and 12.5 µg/mL, respectively, in cytotoxicity evaluations conducted on primary L929 fibroblast cells. This data enabled the determination of the toxic thresholds for L929 fibroblasts associated with Cu@CQDs and CQDs (Fig. 4).

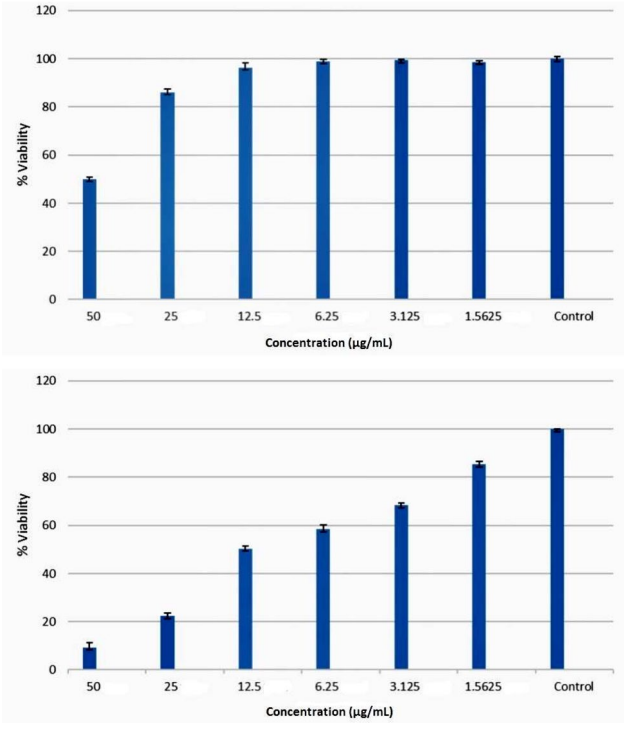

Fig. 4 The L929 fibroblast viability determined by MTT assay following treatment with Cu@CQDs (above) and CQDs (bottom) for 24 h

Effects of CQDs on strongyle eggs and larvae

This study aimed to investigate the effects of CQDs and Cu@CQDs on the hatching of strongyle eggs (Fig. 5) and the behavior of larvae. The hatching experiment involved 100 eggs per concentration, including a positive control group treated with Ivermectin (1%), a negative control group with deionized water, and treatment groups with CQDs and Cu@CQDs at concentrations of 12.5, 6.25, 3.125, and 1.5625 µg/ml. After a 48-hour incubation period at 27 °C, the hatching rates were assessed. The negative control group exhibited a high hatching rate of 92%, with only 8 out of 100 eggs remaining unhatched, while the positive control group showed a significantly reduced hatching rate of 3%. In the CQDs treatment group, the percentage of eggs that did not hatch was 89%, 72%, 57%, and 44% at the respective concentrations. Similarly, the Cu@CQDs treatment group demonstrated hatching inhibition, with 95%, 79%, 69%, and 48% of eggs remaining unhatched at the same concentrations (Table 1). All experiments were performed in triplicate, and average results were used for analysis.

In addition to egg hatching, the feeding behavior of L1 was evaluated. Typically, L1 larvae feed on *Escherichia coli* containing acridine orange [63], which can be visualized under a fluorescent microscope. In the negative control group, *Escherichia coli* was clearly observed in the digestive tract of L1. In contrast, the positive control group (Ivermectin 1%) showed no feeding, as *Escherichia coli* was absent from the larvae's digestive system. In the treatment groups, the fluorescent properties of CQDs allowed for their visualization within the larvae, indicating a lack of nutrient intake (Fig. 6).

In the CQDs treatment group, the number of L1 that did not feed on *Escherichia coli* was 101, 91, 76, and 53 at concentrations of 12.5, 6.25, 3.125, and 1.5625 µg/ml, respectively. For the Cu@CQDs treatment group, the corresponding numbers were 111, 99, 83, and 58 L1 (Fig. 7). A total of 120 L1 were used in each group, and all experiments were conducted in triplicate.

The viability of L3 was also assessed in this study. The experiments included treatment groups with CQDs (G1p) and Cu@CQDs (G1d), as well as control groups: a negative control (G2) and a positive control (G3). The number of live and dead larvae was determined using an optical microscope (Fig. 8), with motility serving as an indicator of viability. Untreated larvae displayed active movement, while those exposed to CQDs and Ivermectin exhibited reduced locomotion and bending frequencies. The results indicated that in group G1p, the number of dead larvae was 104, 93, 80, and 55 at concentrations of 12.5, 6.25, 3.125, and 1.5625 µg/ml, respectively. In group

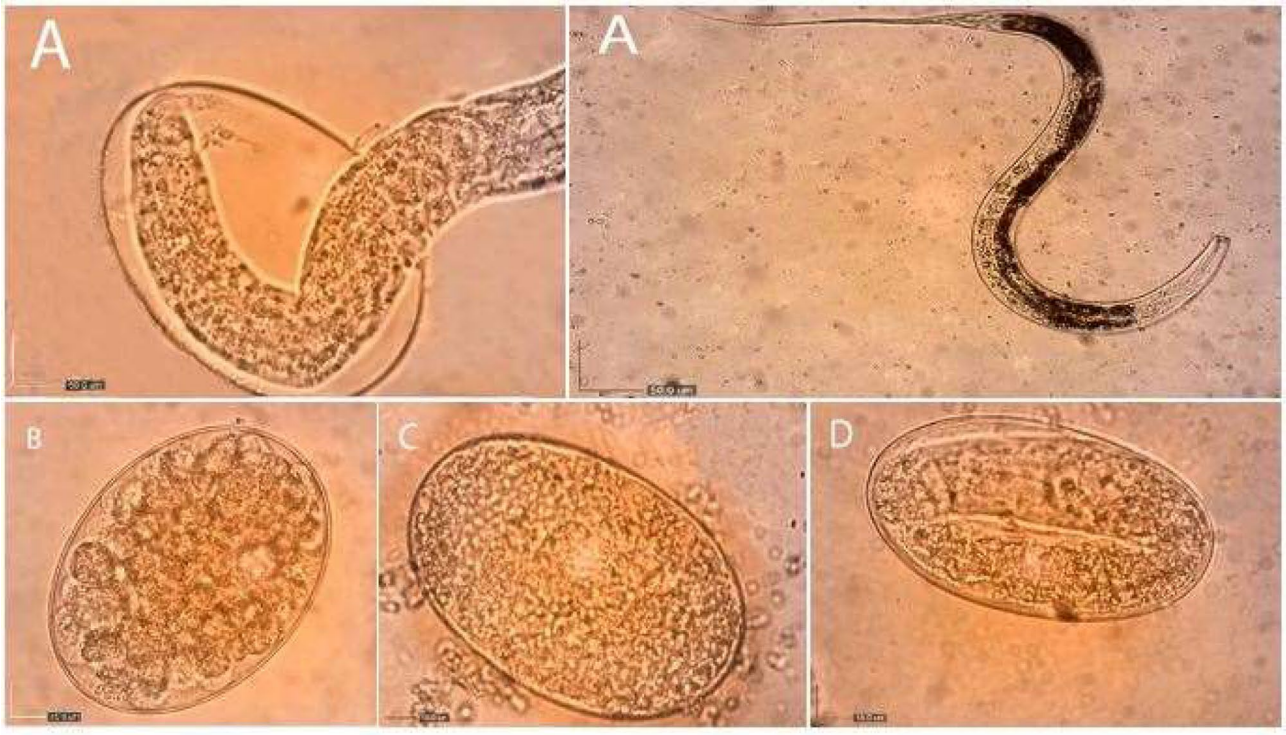

Fig. 5 Strongyle eggs after exposure to negative control group (**A**). (converted to L1), positive control group (**B**). Cu@CQDs (**C**) and CQDs (**D**). Images were captured at 40x magnification

Table 1 Percentage of EHI, LFI, and L3 larvicidal activity in treatment, negative control, and positive control groups). P-value < 0.05)

Treatment	Concentration (µg/ml)	EHI (%)	LFI (%)	L3 Larvicidal Activity (%)
Cu@CQDs	12.5	95	92.5	95
	6.25	79	82.5	85.8
	3.125	69	69.1	71.6
	1.5625	48	48.3	49.1
CQDs	12.5	89	84.1	86.6
	6.25	72	75.8	77.5
	3.125	57	63.3	66.6
	1.5625	44	44.1	45.8
Negative control group	-	8	6.6	5
Positive control group	-	97	95.8	97.5

G1d, the corresponding numbers of dead larvae were 114, 103, 86, and 59. In the control groups, G2 and G3, the number of dead larvae was 6 and 117, respectively (Fig. 7). Each experiment involved a total of 120 L3, and all experiments were conducted in triplicate (Fig. 9).

Assessment of oxidative/nitrosative stress parameters

The incubation of the parasite with both CQDs and Cu@CQDs at varying concentrations (12.5, 6.25, 3.125, and 1.5625 µg/ml) resulted in significant alterations in oxidative and nitrosative stress biomarkers. Notably, both CQDs and Cu@CQDs demonstrated a concentration-dependent increase in MDA levels. At the highest concentration of 12.5 µg/ml, MDA levels increased approximately fivefold compared to the negative controls. In addition to MDA, the TAS was significantly affected by the treatments. Both CQDs and Cu@CQDs led to a marked suppression of TAS, with the addition of 12.5 µg/ml resulting in a reduction of TAS content by up to threefold compared to the negative controls. Furthermore, incubation with 12.5 µg/ml of both CQDs and Cu@CQDs also resulted in elevated PCO levels (Table 2).

Oxidative DNA damage

The assessment of oxidative DNA damage was conducted qualitatively. Under the fluorescent microscope, Group 1 (Cu@CQDs) exhibited a pronounced green color emission, indicating significant DNA damage in the larvae. In contrast, the control group displayed minimal green color emission, suggesting no observable DNA damage. Group 2 (CQDs) also showed green color emission, but at a lower intensity compared to Group 1 (Fig. 10). Consequently, it can be deduced that the DNA damage to the larvae was more severe in the presence of Cu@CQDs.

Ultrastructural analysis

In this study, we employed SEM to investigate the effects of CQDs and Cu@CQDs on strongyle third-stage larvae

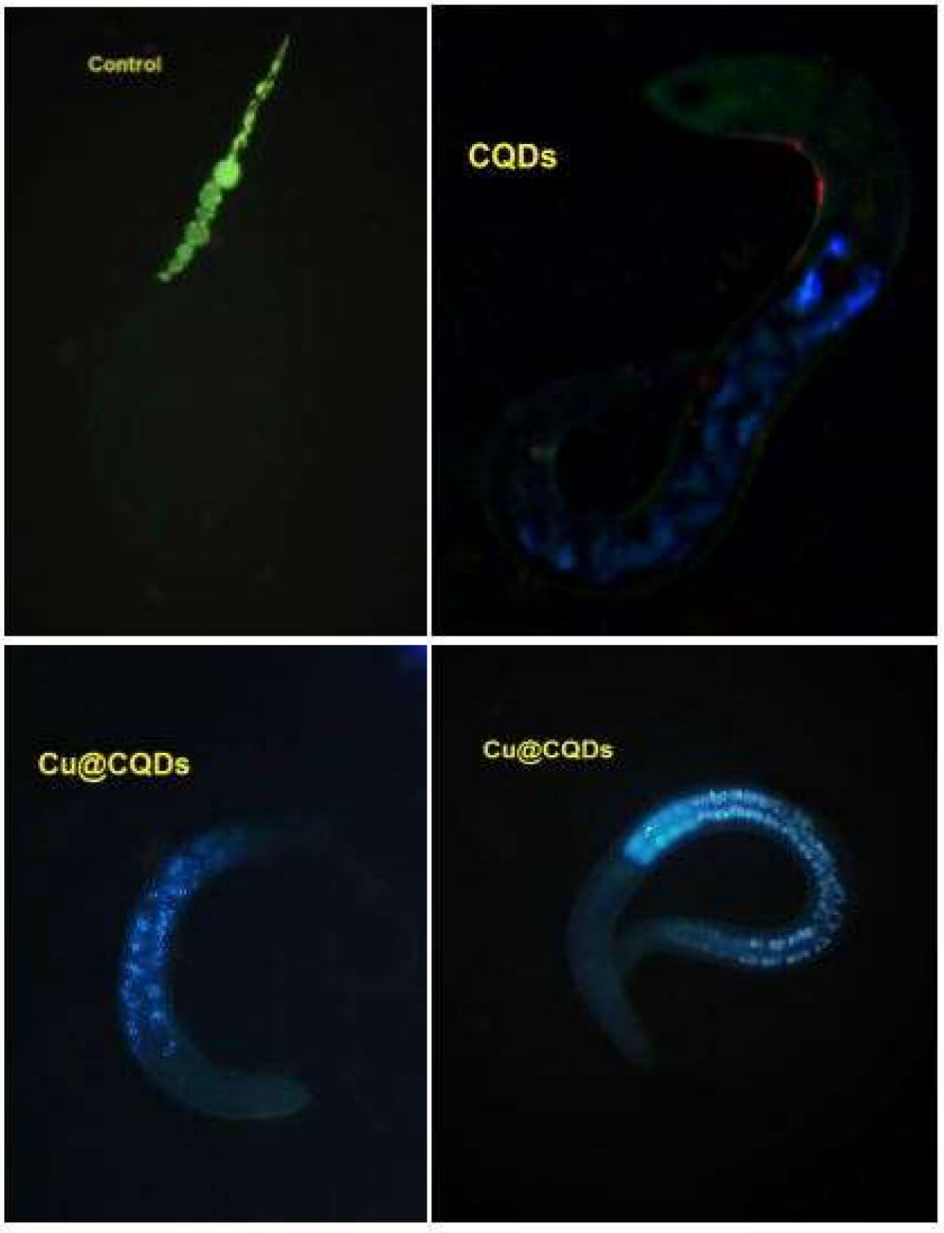

Fig. 6 *E. coli* containing acridine orange in the digestive tract of L1 (control). Cu@CQDs in the digestive tract of L1 (Cu@CQDs). *E. coli* containing acridine orange and CQDs in the digestive tract of L1 (CQDs)

and eggs. The concentrations tested included 12.5, 6.25, 3.125, and 1.5625 µg/ml. For comparison, we also imaged the larvae and eggs from both positive and negative control groups. Our results revealed that exposure to CQDs resulted in significant structural alterations in both the larvae and eggs. Notably, we observed the accumulation of CQDs on and around the surface of the larvae, which led to a disruption of their cuticle structure. Additionally, deformities were noted in the eggs following CQD exposure (Figs. 11 and 12).

Discussion

Despite a dearth of research on the impact of CQDs on nematodes, this investigation represents a pioneering study exploring the antiparasitic potential of CQDs against strongyle larvae and eggs. The data obtained suggest that CQDs exhibit a substantial detrimental impact on the viability of strongyle eggs and L3 stages. The percentage of EHI in Cu@CQDs was higher than that of CQDs, with the highest EHI observed at a concentration of 12.5 µg/ml. The EHI values in the negative and positive control groups were 8% and 97%, respectively. The results suggest that Cu@CQDs have a significant inhibitory

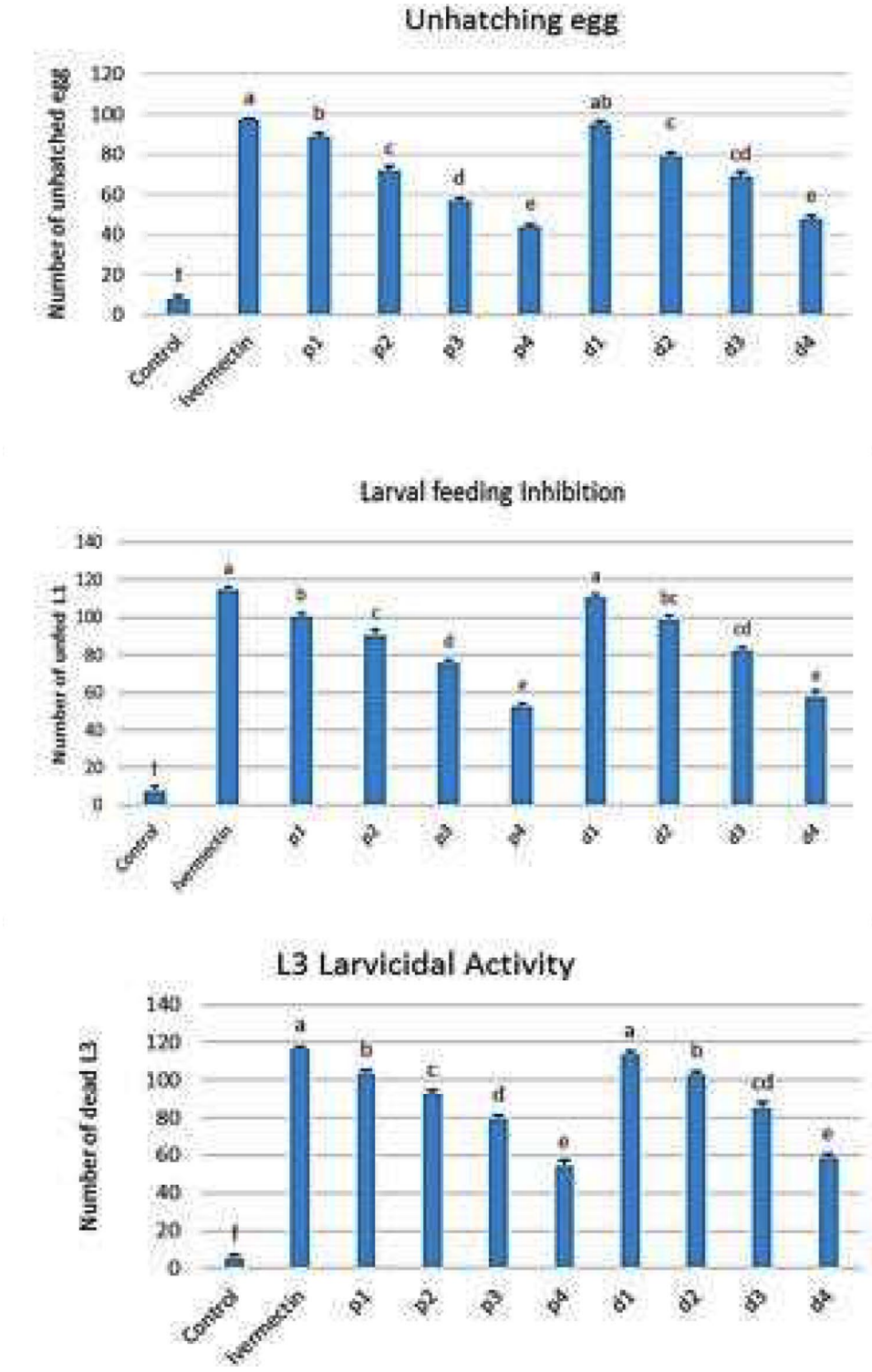

Fig. 7 Number of unhatched strongyle eggs, unfed L1 and mortality rate of L3 after exposure to negative control group, positive control group, and treatment groups. (P1 = CQDs at a concentration of 12.5 µg/ml, P2 = CQDs at a concentration of 6.25 µg/ml, P3 = CQDs at a concentration of 3.125 µg/ml, P4 = CQDs at a concentration of 1.5625 µg/ml, D1 = Cu@CQDs at a concentration of 12.5 µg/ml, D2 = Cu@CQDs at a concentration of 6.25 µg/ml, D3 = Cu@CQDs at a concentration of 3.125 µg/ml, D4 = Cu@CQDs at a concentration of 1.5625 µg/ml. P-value < 0.05)

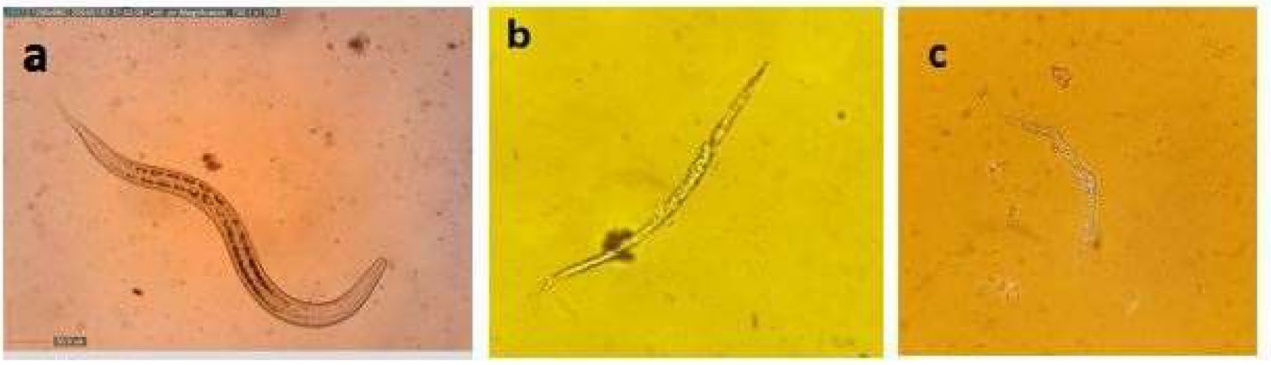

Fig. 8 Photomicrograph of a normal larva (**a**); and those exposed to CQDs (**b**) and Cu@CQDs (**c**) (10x magnification)

Fig. 9 The presence of CQDs inside the digestive tract of L3 under a fluorescent microscope (10x magnification)

effect on the hatching of strongyle eggs. Based on Fig. 7, it can be observed that the positive control group (Ivermectin) and the d1 group (Cu@CQDs at a concentration of 12.5 µg/ml) exhibit similar effects in preventing the hatching of strongyle eggs, indicating that both can demonstrate significant inhibitory effects. Furthermore, it is evident that the treatment group with Cu@CQDs (d) performs better compared to the treatment group with CQDs (p), as they have prevented a greater number of eggs from hatching. Based on the observations made through light microscopy and SEM (Figs. 5 and 11), it is plausible to suggest that the inhibition of egg hatching in the experimental groups was likely due to the accumulation of CQDs around the eggs, which is associated with deformities in the eggs. The eggs treated with CQDs exhibited a predominantly liquid composition, accompanied by small, irregularly shaped morula cells. Furthermore, the larvae developing within these eggs displayed aberrant morphology, characterized by compacted and wrinkled structures. In contrast, the control group depicted a typical developmental progression, with larvae undergoing normal growth stages and successfully hatching from the egg (Fig. 5A).

This study represents a pioneering investigation into the antiparasitic potential of CQDs against strongyle larvae and eggs, addressing a significant gap in the current literature. Our findings indicate that CQDs, particularly those modified with copper (Cu@CQDs), exhibit a substantial detrimental impact on the viability of strongyle eggs and L3 stages. The enhanced efficacy of Cu@CQDs at a concentration of 12.5 µg/ml, which resulted in an EHI comparable to that of the positive control (Ivermectin), aligns with previous studies that have demonstrated the potential of nanoparticles in parasitic control [64].

The observed morphological changes in the eggs and larvae, including deformities and abnormal structures, suggest that CQDs may disrupt normal developmental processes [65]. Dong et al. reported that biomass-based CQDs can induce stress responses in plant systems, which may be analogous to the oxidative stress observed

Table 2 The effect of various concentrations of CQDs and Cu@CQDs on oxidative/nitrosative stress parameters) P-value < 0.05)

test	Control(–)	Cu@CQDs			CQDs				
		1.5625 µg/ml	3.125 µg/ml	6.25 µg/ml	12.5 µg/ml	1.5625 µg/ml	3.125 µg/ml	6.25 µg/ml	12.5 µg/ml
PCO (nmol/mg Pro)	1.09 ± 0.16^{d}	1.18 ± 0.10^{d}	2.88 ± 0.08^{c}	6.39 ± 0.25^{b}	8.11 ± 0.15^{a}	1.12 ± 0.11^{d}	2.46 ± 0.22^{c}	5.92 ± 0.32^{b}	7.94 ± 0.26^{a}
TAS (µmol/mg Pro)	9.28 ± 0.21^{a}	8.82 ± 0.47^{a}	7.11 ± 0.21^{b}	4.02 ± 0.74^{c}	3.24 ± 0.07^{c}	9.14± 0.11^{a}	7.32± 0.28^{ab}	4.52 ± 0.14^{c}	3.61 ± 0.27^{c}
MDA (nmol/mg Pro)	1.73 ± 0.07^{d}	1.96 ± 0.21^{d}	2.74 ± 0.16^{d}	7.71 ± 0.08^{c}	10.21 ± 0.13^{a}	1.85 ± 0.15^{d}	2.51 ± 0.24^{d}	7.11± 0.27^{c}	9.14 ± 0.18^{b}

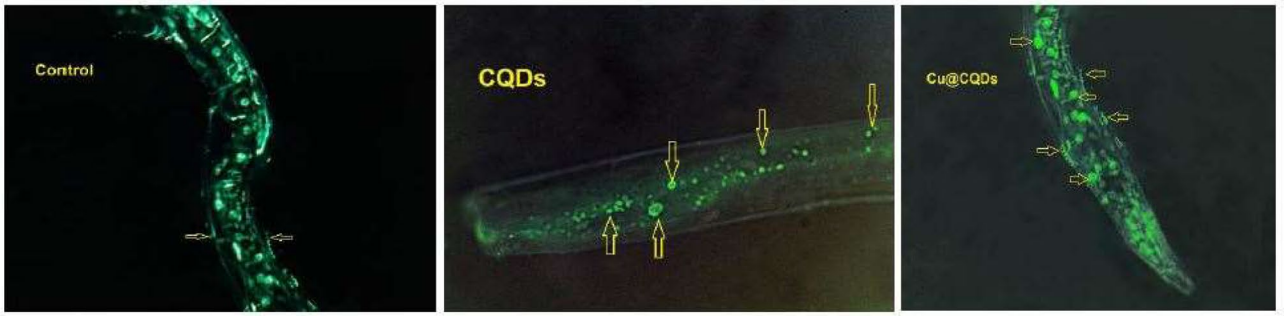

Fig. 10 Fluorescent microscope analysis for immunoreactivity of 8-oxodG (a biomarker of oxidative DNA damage) in larvae longitudinal section. Longitudinal section of larvae: See increased green reactions representing positive reaction against 8-oxodG in CQDs-received groups compared to the control group

in our study. The accumulation of CQDs around the eggs likely interferes with their integrity, resulting in the liquid composition and irregular morula cells we observed.

Furthermore, the highest larval mortality rate of L3 at 12.5 µg/ml in the Cu@CQDs treatment group suggests a dose-dependent relationship, which is supported by the literature on the effects of nanoparticles on nematodes [66]. The deleterious effects on the cuticle and digestive system of the larvae, as evidenced by our analyses based on the microscopic images obtained through fluorescent and SEM (Figs. 9 and 12), indicate that CQDs may exert their antiparasitic effects through mechanisms similar to those reported for other nanoparticles, which often involve oxidative stress and damage to cellular structures [67]. Despite the limited research on the impact of CQDs on nematodes, most studies on nanotechnology in this context have focused on nanoparticles. Given the similarities between nanoparticles and CQDs, and the established anti-parasitic properties of nanoparticles, this study's findings suggest that CQDs may also possess anti-parasitic activity, including anti-larval and anti-egg effects [27].

The results obtained from the study demonstrated that the inhibitory effect on the feeding of L1 was greater in the second treatment group (Cu@CQDs) compared to the first treatment group (CQDs). The highest degree of inhibition was achieved at a concentration of 12.5 µg/ml in the second treatment group (Table 1), likely attributed to the presence of copper in the structure of CQDs. Moreover, the absence of feeding in first-stage larvae of *Escherichia coli* containing acridine orange following exposure to Ivermectin 1% (positive control group) was attributed to the development of pharyngeal paralysis in this stage of larvae. Furthermore, the presence of copper in the structure of Cu@CQDs prevented the feeding of first-stage larvae through the same mechanism [68].

Our results also demonstrate that both CQDs and Cu@CQDs induce oxidative stress, as indicated by increased levels of MDA and PCO. This finding is in line with the prevailing notion that the toxic effects of CQDs are mediated by the generation of reactive oxygen species (ROS), which can lead to significant cellular damage [66]. Conversely, consuming antioxidants appeared to reduce oxidative damage, as indicated by decreased TAS levels. These findings are consistent with previous reports, which likely provide support and validation for the observed results [1, 69]. As previously reported, the prevailing notion is that the primary mechanism underlying the toxic effects of CQDs involves the induction of oxidative stress and the generation of reactive oxygen species (ROS), which can damage lipids, carbohydrates, proteins, and DNA [70]. The larvae that received CQDs showed a dose-dependent increase in levels of PCO and MDA, as well as immunoreactivity of 8-oxodG and DNA damage. These alterations are indicative of oxidative stress-induced damage [50]. Notably, the exacerbation of oxidative stress in larvae treated with Cu@CQDs suggests that the presence of copper may enhance the toxic effects, corroborating the findings of previous studies

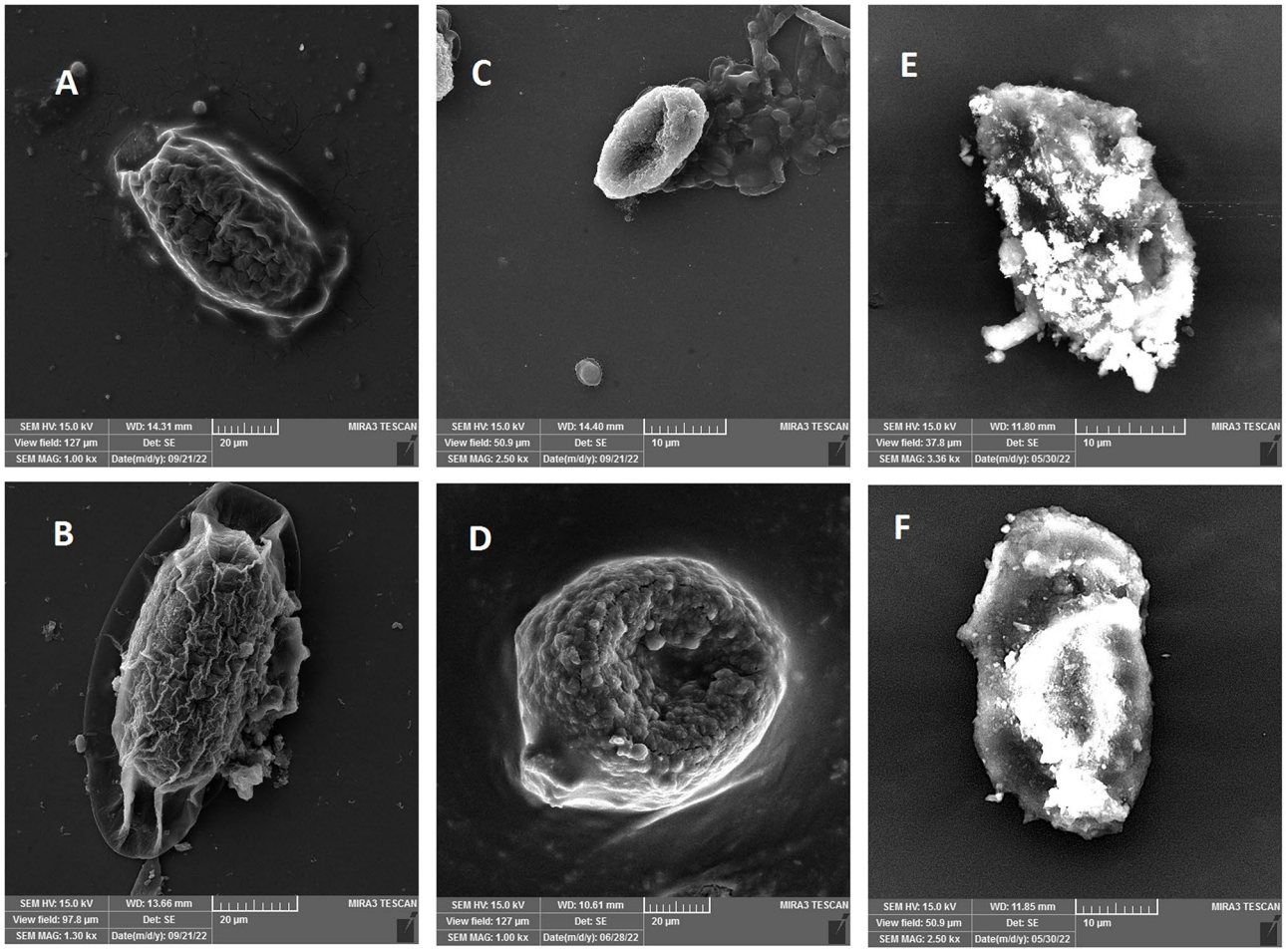

Fig. 11 SEM image of strongyle egg after exposure to negative control group (**A & B**), CQDs (**C & D**), Cu@CQDs (**E & F**)

that have linked metal nanoparticles to increased oxidative damage [64].

It is indeed conceivable that the small size of CQDs allows them to penetrate the eggshell and larval cuticle, potentially increasing lethality [27]. This study is the first to utilize SEM to demonstrate the effects of CQDs on strongyle eggs and larvae, marking a significant advancement in our understanding of their antiparasitic properties.

Based on the findings and analyses conducted, it is evident that Cu@CQDs at a concentration of 12.5 µg/ml exhibit notable antiparasitic efficacy, suggesting their potential as a viable alternative to conventional antiparasitic medications. Further investigation is necessary to ascertain the specific mechanism of action of CQDs in combatting nematodes like strongyle.

Considering the size and high permeability of CQDs, as well as their relative novelty, there is a potential risk of environmental damage associated with their use. This underscores the necessity for further research in this area. However, existing studies indicate that, in addition to their antiparasitic properties, CQDs exhibit significant environmental friendliness, as they do not produce harmful effects during biodegradation. This characteristic not only enhances their suitability for veterinary applications but also aligns with the growing demand for sustainable and eco-friendly alternatives in pest management. Therefore, the application of CQDs may represent a promising strategy for controlling nematode populations while minimizing ecological impact [65].

Conclusion

This study provides compelling evidence for the potential of CQDs and Cu@CQDs as effective alternatives to conventional anthelmintics in the control of strongyle nematodes. The increasing prevalence of resistance to traditional treatments, such as Ivermectin, underscores the urgent need for innovative solutions in veterinary parasitology. Our research findings not only demonstrate the nematicidal properties of CQDs and Cu@CQDs but also highlight their multifaceted mechanisms of action, including the induction of oxidative stress and significant morphological alterations in nematodes.

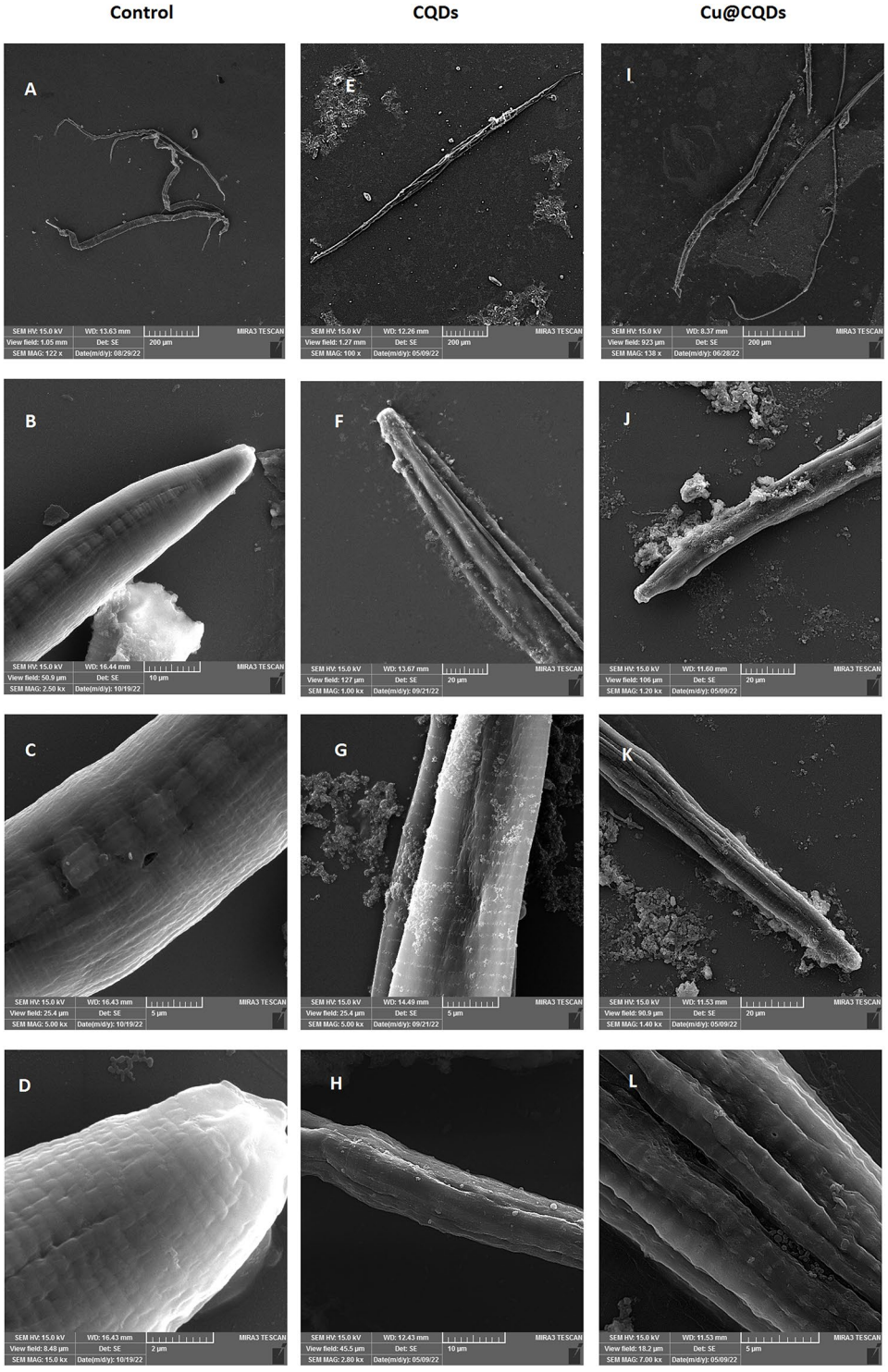

Fig. 12 SEM image of strongyle L3 after exposure to negative control group (**A-D**), CQDs (**E-H**), Cu@CQDs (**I-L**)

Specifically, the anthelmintic properties of Cu@CQDs exhibit a concentration-dependent relationship, with the highest dosage (12.5 µg/ml) demonstrating significant inhibitory effects on the antioxidant systems of the nematodes, leading to damage to biomolecules such as lipids, proteins, and DNA. Furthermore, our results suggest that Cu@CQDs may penetrate the cuticles of larvae, while CQDs have been found to exert anthelmintic effects within the internal structure of the larvae's digestive system, potentially disrupting the parasite's nutrient uptake

and absorption. The ability of Cu@CQDs to achieve high levels of EHI and larval motility impairment indicates that these nanomaterials could serve as viable candidates for future antiparasitic therapies. Their unique properties, including small size and high surface area, facilitate penetration into nematode structures, thereby enhancing their efficacy. Additionally, CQDs have been shown to induce pharyngeal paralysis in L1, compromising the worms' ability to feed and survive. The observed oxidative stress markers suggest that CQDs may disrupt cellular integrity, leading to increased mortality rates in treated larvae. This mechanism of action aligns with the growing body of literature supporting the use of nanomaterials in combating parasitic infections.

Despite these promising results, it is essential to acknowledge the limitations of this study, particularly the in vitro nature of the experiments, which may not fully replicate the complexities of in vivo environments. Therefore, further research is warranted to evaluate the safety, efficacy, and potential side effects of CQDs and Cu@CQDs in live animal models. Investigations into the long-term environmental impacts of these nanomaterials are also crucial, as their widespread application could have unforeseen ecological consequences.

Collectively, these findings suggest that Cu@CQDs possess significant potential as an effective and promising substitute for chemical nematicides. In light of these results, it is evident that CQDs and Cu@CQDs represent a substantial advancement in the search for sustainable and effective alternatives to traditional anthelmintics. Their application could enhance the management of strongyle infections in livestock and contribute to the broader goal of reducing reliance on conventional drugs that are increasingly compromised by resistance.

Supplementary Information

The online version contains supplementary material available at https://doi.org/10.1186/s12917-025-04494-5.

Supplementary Material 1

Acknowledgements
The authors would like to sincerely thank the members of the Faculty of Veterinary Medicine and Urmia University Research Council for the approval and support of this research. We are also grateful to Dr. Awat Samiei for his technical assistance.

Author contributions
Armin Fakheri: Investigation, Methodology, Writing – original draft. Bijan Esmaeilnejad: Conceptualization, Methodology, Formal analysis, Writing – review & editing. Hamid Akbari: Supervision, Visualization. Rahim Molaei: Conceptualization, Methodology, Formal analysis, Writing – review & editing.

Funding
This research has been financially supported by Research Council of Urmia University.

Data availability
no comments.

Declarations

Ethics approval and consent to participate
All of the protocols were approved by the Faculty of Veterinary Medicine's Committee on the Ethics of Animal Experiments at Urmia University (IR-UU-AEC-3/73). Every procedure was carried out in accordance with the relevant laws and standards. The study was conducted in compliance with the ARRIVE standards. The owner(s) of the animals gave their informed consent for us to use them in the study.

Consent to participate
Not applicable.

Consent to publish
Not applicable.

Competing interests
The authors declare no competing interests.

Author details
[1]Department of Pathobiology, Faculty of Veterinary Medicine, Urmia University, Urmia, Iran
[2]Department of Clinical Sciences, Faculty of Veterinary Medicine, University of Tabriz, Tabriz, Iran
[3]Materials Synthesis Laboratory, Carbon Tech Industrial Group, Carbon Tech, Tehran, Iran

Received: 16 September 2024 / Accepted: 14 January 2025
Published online: 22 January 2025

References

1. Esmaeilnejad B, Samiei A, Mirzaei Y, Farhang-Pajuh F. Assessment of oxidative/nitrosative stress biomarkers and DNA damage in Haemonchus Contortus, following exposure to zinc oxide nanoparticles. Acta Parasitol. 2018;63(3):563–71.
2. Roeber F, Jex AR, Gasser RB. Impact of gastrointestinal parasitic nematodes of sheep, and the role of advanced molecular tools for exploring epidemiology and drug resistance-an Australian perspective. Parasites Vectors. 2013;6:1–13.
3. Vidyashankar A, Hanlon B, Kaplan R. Statistical and biological considerations in evaluating drug efficacy in equine strongyle parasites using fecal egg count data. Vet Parasitol. 2012;185(1):45–56.
4. Love S, Murphy D, Mellor D. Pathogenicity of cyathostome infection. Vet Parasitol. 1999;85(2–3):113–22.
5. Matthews J, Hodgkinson J, Dowdall S, Proudman C. Recent developments in research into the Cyathostominae and Anoplocephala Perfoliata. Vet Res. 2004;35(4):371–81.
6. Nielsen M, Reinemeyer C, Donecker J, Leathwick D, Marchiondo A, Kaplan R. Anthelmintic resistance in equine parasites—current evidence and knowledge gaps. Vet Parasitol. 2014;204(1–2):55–63.
7. Geurden T, Hoste H, Jacquiet P, Traversa D, Sotiraki S, di Regalbono AF, Tzanidakis N, Kostopoulou D, Gaillac C, Privat S. Anthelmintic resistance and multidrug resistance in sheep gastro-intestinal nematodes in France, Greece and Italy. Vet Parasitol. 2014;201(1–2):59–66.
8. Allison K, Taylor NM, Wilsmore A, Garforth C. Equine anthelmintics: survey of the patterns of use, beliefs and attitudes among horse owners in the UK. Vet Rec. 2011;168(18):483–483.
9. Nielsen M, Monrad J, Olsen S. Prescription-only anthelmintics—a questionnaire survey of strategies for surveillance and control of equine strongyles in Denmark. Vet Parasitol. 2006;135(1):47–55.
10. Peregrine AS, Molento MB, Kaplan RM, Nielsen MK. Anthelmintic resistance in important parasites of horses: does it really matter? Vet Parasitol. 2014;201(1–2):1–8.
11. Jhonsi MA, Ananth DA, Nambirajan G, Sivasudha T, Yamini R, Bera S, Kathiravan A. Antimicrobial activity, cytotoxicity and DNA binding studies of carbon dots. Spectrochim Acta Part A Mol Biomol Spectrosc. 2018;196:295–302.

12. Zuo P, Lu X, Sun Z, Guo Y, He H. A review on syntheses, properties, characterization and bioanalytical applications of fluorescent carbon dots. Microchim Acta. 2016;183:519–42.
13. Zhao A, Chen Z, Zhao C, Gao N, Ren J, Qu X. Recent advances in bioapplications of C-dots. Carbon. 2015;85:309–27.
14. Song-Ling Y, HUANG J-J, Lin L, Hui-Jun F, Yuan-Ming S, Yu-Dong S, Hong-Tao L, Zhen-Lin X. Preparation of carbon dots and their application in food analysis as signal probe. Chin J Anal Chem. 2017;45(10):1571–81.
15. Zhang J, An X, Li X, Liao X, Nie Y, Fan Z. Enhanced antibacterial properties of the bracket under natural light via decoration with ZnO/carbon quantum dots composite coating. Chem Phys Lett. 2018;706:702–7.
16. Moradi M, Molaei R, Kousheh SA, Guimarães T, McClements J. Carbon dots synthesized from microorganisms and food by-products: active and smart food packaging applications. Crit Rev Food Sci Nutr. 2023;63(14):1943–59.
17. Shi X, Wang X, Zhang S, Zhang Z, Meng X, Liu H, Qian Y, Lin Y, Yu Y, Lin W. Hydrophobic carbon dots derived from organic pollutants and applications in NIR anticounterfeiting and bioimaging. Langmuir. 2023;39(14):5056–64.
18. Zhang L, Yang X, Yin Z, Sun L. A review on carbon quantum dots: synthesis, photoluminescence mechanisms and applications. Luminescence. 2022;37(10):1612–38.
19. Shahshahanipour M, Rezaei B, Ensafi AA, Etemadifar Z. An ancient plant for the synthesis of a novel carbon dot and its applications as an antibacterial agent and probe for sensing of an anti-cancer drug. Mater Sci Engineering: C. 2019;98:826–33.
20. Li H, Huang J, Song Y, Zhang M, Wang H, Lu F, Huang H, Liu Y, Dai X, Gu Z. Degradable carbon dots with broad-spectrum antibacterial activity. ACS Appl Mater Interfaces. 2018;10(32):26936–46.
21. Dong X, Liang W, Meziani MJ, Sun Y-P, Yang L. Carbon dots as potent antimicrobial agents. Theranostics. 2020;10(2):671.
22. Priyadarshini E, Rawat K, Prasad T, Bohidar H. Antifungal efficacy of Au@ carbon dots nanoconjugates against opportunistic fungal pathogen, Candida albicans. Colloids Surf B. 2018;163:355–61.
23. Bagheri Z, Ehtesabi H, Hallaji Z, Aminoroaya N, Tavana H, Behroodi E, Rahimifard M, Abdollahi M, Latifi H. On-chip analysis of carbon dots effect on yeast replicative lifespan. Anal Chim Acta. 2018;1033:119–27.
24. Ferraz CM, Silva LPC, de Freitas Soares FE, Souza RLO, Tobias FL, de Araújo JV, Veloso FBR, Laviola FP, Endringer DC, de Gives PM. Effect of silver nanoparticles (AgNP's) from Duddingtonia flagrans on cyathostomins larvae (subfamily: cyathostominae). J Invertebr Pathol. 2020;174:107395.
25. Kumar VB, Dolitzky A, Michaeli S, Gedanken A. Antiparasitic ointment based on a biocompatibile carbon dot nanocomposite. ACS Appl Nano Mater. 2018;1(4):1784–91.
26. Zhu P-p, Cheng Z, Du L-l, Chen Q, Tan K-j. Synthesis of the Cu-doped dual-emission fluorescent carbon dots and its analytical application. Langmuir. 2018;34(34):9982–9.
27. Samiei A, Tavassoli M, Esmaeilnejad B. Green synthesis and anthelmintic activity of silver nanoparticles using Morus Alba Fruit extract against different stages of equine strongyles. Vet Res Commun 2024:1–16.
28. Buza V, Cătană L, Andrei S, Ștefănuț L, Răileanu Ș, Matei M, Vlasiuc I, Cernea M. In vitro anthelmintic activity assessment of six medicinal plant aqueous extracts against donkey strongyles. J Helminthol. 2020;94:e147.
29. Lejeune M, Mann S, White H, Maguire D, Hazard J, Young R, Stone C, Antczak D, Bowman D. Evaluation of Fecal Egg count tests for Effective Control of Equine Intestinal Strongyles. Pathogens. 2023;12(11):1283.
30. Thienpont D, Rochette F, Vanparijs OFJ. Diagnosing helminthiasis by coprological examination. 1986.
31. Braga FR, Araujo JV, Silva AR, Araujo JM, Carvalho RO, Tavela AO, Campos AK, Carvalho GR. Biological control of horse cyathostomin (Nematoda: Cyathostominae) using the nematophagous fungus Duddingtonia flagrans in tropical southeastern Brazil. Vet Parasitol. 2009;163(4):335–40.
32. Amer MM, Desouky A, Helmy NM, Abdou AM, Sorour SS. Identifying 3rd larval stages of common strongylid and non-strongylid nematodes (class: Nematoda) infecting Egyptian equines based on morphometric analysis. BMC Vet Res. 2022;18(1):432.
33. Ghimire TR, Bhattarai N. A survey of gastrointestinal parasites of goats in a goat market in Kathmandu, Nepal. J Parasitic Dis. 2019;43(4):686–95.
34. Coles G, Bauer C, Borgsteede F, Geerts S, Klei T, Taylor M, Waller P. World Association for the Advancement of Veterinary Parasitology (WAAVP) methods for the detection of anthelmintic resistance in nematodes of veterinary importance. Vet Parasitol. 1992;44(1–2):35–44.
35. Zak A, Siwinska N, Slowikowska M, Borowicz H, Kubiak K, Hildebrand J, Popiolek M, Niedzwiedz A. Searching for ivermectin resistance in a Strongylidae population of horses stabled in Poland. BMC Vet Res. 2017;13:1–5.
36. Peachey L, Pinchbeck G, Matthews J, Burden F, Behnke J, Hodgkinson J. Papaya latex supernatant has a potent effect on the free-living stages of equid cyathostomins in vitro. Vet Parasitol. 2016;228:23–9.
37. De Jesús-Martínez X, Olmedo-Juárez A, Olivares-Pérez J, Zamilpa A, Mendoza de Gives P, López-Arellano M, Rojas-Hernández S, Villa-Mancera A, Camacho-Díaz L, Cipriano-Salazar M. In vitro anthelmintic activity of methanolic extract from Caesalpinia coriaria J. Willd fruits against Haemonchus Contortus eggs and infective larvae. Biomed Res Int. 2018;2018(1):7375693.
38. Geary TG, SIMs SM, THoMAs EM, Vanover L, Davis J, Winterrowd C, Klein R, Ho N, Thompson D. Haemonchus contortus: ivermectin-induced paralysis of the pharynx. Exp Parasitol. 1993;77(1):88–96.
39. Matthews JB, McArthur C, Robinson A, Jackson F. The in vitro diagnosis of anthelmintic resistance in cyathostomins. Vet Parasitol. 2012;185(1):25–31.
40. Thambiraj S, Shankaran R. Green synthesis of highly fluorescent carbon quantum dots from sugarcane bagasse pulp. Appl Surf Sci. 2016;390:435–43.
41. Neeraja M, Lakshmi V, Padmasri C, Padmaja K. Utility of Acridine Orange staining for detection of bacteria from positive blood cultures. J Microbiol Methods. 2017;139:215–7.
42. Diekmann I, Blazejak K, Krücken J, Strube C, von Samson-Himmelstjerna G. Comparison of morphological and molecular Strongylus spp. identification in equine larval cultures and first report of a patent Strongylus asini infection in a horse. Equine Vet J 2024.
43. Staniland L. A modification of the Baermann funnel technique for the collection of nematodes from plant material. J Helminthol. 1954;28(1–2):115–8.
44. Barbosa ACMS, Silva LPC, Ferraz CM, Tobias FL, de Araújo JV, Loureiro B, Braga GMAM, Veloso FBR, Soares FEF, Fronza M. Nematicidal activity of silver nanoparticles from the fungus Duddingtonia flagrans. Int J Nanomed 2019:2341–8.
45. Al-Rofaai A, Rahman W, Abdulghani M. Sensitivity of two in vitro assays for evaluating plant activity against the infective stage of Haemonchus contortus strains. Parasitol Res. 2013;112:893–8.
46. Hadaś E, Stankiewicz M. Superoxide dismutase and total antioxidant status of larvae and adults of Trichostrongylus Colubriformis, Haemonchus Contortus and Ostertagia Circumcincta. Parasitol Res. 1998;84:646–50.
47. Ding AH, Nathan CF, Stuehr D. Release of reactive nitrogen intermediates and reactive oxygen intermediates from mouse peritoneal macrophages. Comparison of activating cytokines and evidence for independent production. J Immunol (Baltimore Md: 1950). 1988;141(7):2407–12.
48. Levine N. Veterinary Protozoology, Iowa State Üniv. *Press Ames Iowa* 1985.
49. Buege JA, Aust SD. [30] microsomal lipid peroxidation. Methods in enzymology. Volume 52. edn.: Elsevier; 1978. pp. 302–10.
50. Radmanesh F, Razi M, Shalizar-Jalali A. Curcumin nano-micelle induced testicular toxicity in healthy rats; evidence for oxidative stress and failed homeostatic response by heat shock proteins 70-2a and 90. Biomed Pharmacother. 2021;142:111945.
51. Nuthong P. Utilization of confocal laser scanning microscopy to locate lipid droplets in sweet-dried chicken. Scope J. 2012.
52. Sousa AJ, Souza PF, Gifoni JM, Dias LP, Freitas CD, Oliveira JT, Sousa DO, Vasconcelos IM. Scanning electron microscopy reveals deleterious effects of Moringa oleifera seed exuded proteins on root-knot nematode Meloidogyne incognita eggs. Int J Biol Macromol. 2020;154:1237–44.
53. Mintz KJ, Bartoli M, Rovere M, Zhou Y, Hettiarachchi SD, Paudyal S, Chen J, Domena JB, Liyanage PY, Sampson R. A deep investigation into the structure of carbon dots. Carbon. 2021;173:433–47.
54. Koutamehr ME, Moradi M, Tajik H, Molaei R, Heshmati MK, Alizadeh A. Sour whey-derived carbon dots; synthesis, characterization, antioxidant activity and antimicrobial performance on foodborne pathogens. LWT. 2023;184:114978.
55. Divsalar E, Tajik H, Moradi M, Molaei R. Carbon dot-based antimicrobial photosensitizer: synthesis, characterization and antimicrobial performance against food borne pathogens. Food Bioscience. 2023;56:103220.
56. Ghorbani M, Tajik H, Moradi M, Molaei R, Alizadeh A. One-pot microbial approach to synthesize carbon dots from baker's yeast-derived compounds for the preparation of antimicrobial membrane. J Environ Chem Eng. 2022;10(3):107525.
57. Du J, Zhao Y, Chen J, Zhang P, Gao L, Wang M, Cao C, Wen W, Zhu C. Difunctional Cu-doped carbon dots: catalytic activity and fluorescence indication for the reduction reaction of p-nitrophenol. RSC Adv. 2017;7(54):33929–36.

58. Raul PK, Senapati S, Sahoo AK, Umlong IM, Devi RR, Thakur AJ, Veer V. CuO nanorods: a potential and efficient adsorbent in water purification. RSC Adv. 2014;4(76):40580–7.
59. Reddy KR. Green synthesis, morphological and optical studies of CuO nanoparticles. J Mol Struct. 2017;1150:553–7.
60. Pakbin B, Zolghadr L, Rafiei S, Brück WM, Brück TB. FTIR differentiation based on genomic DNA for species identification of Shigella isolates from stool samples. Sci Rep. 2022;12(1):2780.
61. Sohn JS, Kwon YW, Jin JI, Jo BW. DNA-templated preparation of gold nanoparticles. Molecules. 2011;16(10):8143–51.
62. Rolim T, Cancino J, Zucolotto V. A nanostructured genosensor for the early diagnosis of systemic arterial hypertension. Biomed Microdevices. 2015;17:1–9.
63. Ellegaard-Jensen L, Jensen KA, Johansen A. Nano-silver induces dose-response effects on the nematode Caenorhabditis elegans. Ecotoxicol Environ Saf. 2012;80:216–23.
64. Rehman A, Ullah R, Uddin I, Zia I, Rehman L, Abidi S. In vitro anthelmintic effect of biologically synthesized silver nanoparticles on liver amphistome, Gigantocotyle Explanatum. Exp Parasitol. 2019;198:95–104.
65. Dong Z, Qi J, Yue L, Zhou H, Chen L, Gu J, He Y, Wu H. Biomass-based carbon quantum dots and their agricultural applications. Plant Stress 2024;11:100411.
66. Atchudan R, Edison TNJI, Shanmugam M, Perumal S, Somanathan T, Lee YR. Sustainable synthesis of carbon quantum dots from banana peel waste using hydrothermal process for in vivo bioimaging. Physica E. 2021;126:114417.
67. Tauseef A, Gupta J, Rehman A, Uddin I. Differential response of cowpea towards the CuO nanoparticles under Meloidogyne incognita stress. South Afr J Bot. 2021;139:175–82.
68. Mashock MJ, Zanon T, Kappell AD, Petrella LN, Andersen EC, Hristova KR. Copper oxide nanoparticles impact several toxicological endpoints and cause neurodegeneration in Caenorhabditis elegans. PLoS ONE. 2016;11(12):e0167613.
69. Baghbani Z, Esmaeilnejad B, Asri-Rezaei S. Assessment of oxidative/nitrosative stress biomarkers and DNA damage in Teladorsagia circumcincta following exposure to zinc oxide nanoparticles. J Helminthol. 2020;94:e115.
70. Kohen R, Nyska A. Invited review: oxidation of biological systems: oxidative stress phenomena, antioxidants, redox reactions, and methods for their quantification. Toxicol Pathol. 2002;30(6):620–50.

Publisher's note